



Design Procedure of an Outer Rotor Synchronous Reluctance Machine for Scooter Application

S. R. Salehinia^a, S. E. Afjei^{*a}, A. Hekmati^b, H. Aghazadeh^a

^a Department of Power Electrical Eng., Faculty of Electrical Engineering, University of Shahid Beheshti, Tehran, Iran

^b Electric Machine Research Group Niroo Research Institute

PAPER INFO

Paper history:

Received 21 June 2020

Received in revised form 23 September 2020

Accepted 30 December 2020

Keywords:

Finite Element Method

Magnetic Flux Barrier

Synchronous Reluctance Motor

Torque Ripple

ABSTRACT

Synchronous reluctance motors, despite their cost-effective types and wide range of speed, generally have a considerable torque ripple due to changes in magnetic resistance between the flux barriers and the stator teeth. Given the numerous possible rotor combinations with different forms of flux barriers, designing an optimal synchronous reluctance motor without the use of mathematical equations and a clear algorithm will be very time-consuming. In this study, a comprehensive method is used to design a synchronous reluctance motor with an external rotor and a flux barrier shape adopted from the behavior of fluids around a solid rotor. According to the new topology, an external rotor synchronous reluctance motor is designed. Multi-objective Taguchi optimization algorithm based on finite element analysis (FEM) is used to maximize the average torque and reduce the torque ripple. This motor is designed for 300 W electric scooters with a six-pole rotor, a 36-slot stator, and a distributed winding. Finally, a prototype of the proposed motor is constructed to validate the results of simulations. The experimental results confirm the accuracy of the design method.

doi: 10.5829/ije.2021.34.03c.10

NOMENCLATURE

	Average Torque (N.m)	Greek Symbols	
T_{av}	Average Torque (N.m)	ρ	Mass density (kg/m ³)
<i>SynRM</i>	Synchronous Reluctance Motor	η	Efficiency
<i>EX – SynRM</i>	External rotor Synchronous Reluctance Motor	ψ	potential(m ² /s ²)
TR	Torque ripple	ξ	differential operator with the flow field
FEM	Finite Element Method	ν	Kinematic viscosity (m ² /s)
MMF	Magneto-motive force	μ	viscosity coefficient(kg/(m.s))
g	Air-gap width (mm)	Subscripts	
I	Rated current (A)	k	flux barriers number
f	Average MMF	m	flux barriers number
P_r	Pressure(kg/m ³)	q	along the q-axis
S	Iron parts thickness	d	along the d-axis
N_s	Rated Speed (rpm)		

1. INTRODUCTION

Simplicity the synchronous reluctance motor, with no need for a squirrel cage in the rotor and permanent magnet, and the similarity of its stator production line

with the widely used induction motor [1-4], have attracted the electric motors' designers and manufacturers in recent years. Most studies into the basics of this motor have been carried out on internal rotor models and there are a limited number of articles regarding external rotor architecture [5-9]. However, external rotor electric motors, thanks to their higher torque compared to the internal rotor architecture, have

*Corresponding Author Institutional Email: e-afjei@sbu.ac.ir (S.E Afjei)

more practical applications, especially in electrical vehicles [10, 11].

Limited amounts of studies are conducted in the field of reluctance motor design with external. The proposed method in considers the thickness of the flux barrier to be equal along the flux barrier. The chief reason behind this design is said to be mechanical strength. While it is shown that the closer the flux barrier shape is to the behavior of the flux lines in the rotor, the more optimized the design procedure is discussed in literature [12]. In this paper, the shape of flux barriers is designed based on the fluid-liquid velocity equation. By selecting the appropriate parameters and optimizing, a comprehensive design for the external rotor synchronous motor is presented. The present study intends to introduce a new comprehensive design method for the Ex-SynRM based on the formation in the shape of flux barriers in the solid rotor using its similarity to the pattern of fluid velocity equations around a solid object. To design external rotors in a synchronous reluctance motor (SynRM), it is tried to block the flux along the q-axis and maximize the magnetic conductance along the d-axis [12, 13]. The flux barriers in the rotor are designed in three steps: (i) determining the flux barriers shape using mathematical equations, (ii) barriers placement on the q-axis, and (iii) optimizing the designed rotor. Then, the shape of flux barriers between the d and q axes is determined through defining some equations that depend on the radius and angle of the points on the flux barrier line in the rotor. The flux barriers start from the q-axis and end around the d-axis. All points between the start and endpoints on the flux barrier line have their own radius, angle and a constant parameter (parameter C). Figure 1 depicts a mathematical definition used for the internal rotor in more details are discussed in literature [14,15]. The design is further optimized through the optimization method, so that the closer the shape of the generated flux barriers is to the shape of the flux lines, the higher average torque discussed in literature [14]. The proposed design procedure of the external rotor is shown in Figure 2.

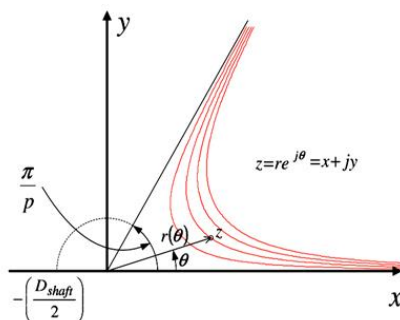


Figure 1. Mathematical definition of the parameters describing the barriers line in a two-pole machine [15]

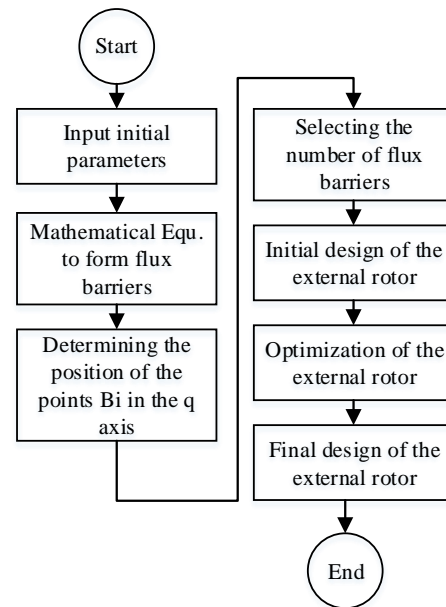


Figure 2. Design procedure of the proposed EX-SynRM

In this regard, this paper presents a new strategy for the design and analysis of EX-SynRM. The contents are organized as follows. The flux barriers shape in the rotor is provided in the second section of the proposed mathematical equations, considering some variables for improvement of the motor performance. Then the variables are evaluated through finite element analysis. In the last part of this section, the number of flux barriers is determined. Section 4 pertains to optimization through Taguchi method taking numerous variables into account. Finally, the proposed design is constructed for an electric scooter and the results of finite element analysis are compared with those of the manufactured motor.

2. MATHEMATICAL APPROACH

As a symmetric Stokes flow around a solid sphere shown in Figure 3a [16], the fluid flow lines around a solid sphere are similar to the magnetic flux lines distribution in Figure 3b. The equations expressing the motion of the fluid, with two properties of adhesion and incompressibility can be expressed as follows [16].

$$\nabla \cdot V = 0 \quad (1)$$

$$\rho \frac{DV}{Dt} = -\nabla Pr + \mu \nabla^2 V \quad (2)$$

$$Pr = pr + \rho \psi \quad (3)$$

where $V(\text{m}^2/\text{s})$ is the liquid instantaneous velocity, $Pr(\text{kg}/\text{m}^3)$ is the liquid natural pressure, $\rho \psi$ is the

gravitational potential energy per unit volume (the combination of these two pressures is known as the effective pressure) Equation (3), ρ is the liquid mass density, μ (kg/(m.s)) is the liquid viscosity coefficient which is calculated experimentally, and ψ (m²/s²) is the gravitational potential [16]. Assume a solid sphere of radius a in the standard spherical coordinates plane with the components r , θ , and ϕ . The fluid flow surrounds the sphere ($r > a$), which is an example of the axial Stokes flow [16]. the symmetric axial Stokes flow, the fluid velocity equation can be considered as follows.

$$V(r) = v_r(r, \theta)e_r + v_\theta(r, \theta)e_\theta \quad (4)$$

According to literature [16] and assuming an incompressible liquid:

$$V = \nabla \phi \times \nabla \psi \quad (5)$$

where $\psi(r, \theta)$ is the Stokes flow function. Then,

$$v_r(r, \theta) = -\frac{1}{r^2 \sin \theta} \frac{\partial \psi(r, \theta, \phi)}{\partial \theta} \quad (6)$$

$$v_\theta(r, \theta) = \frac{1}{r \sin \theta} \frac{\partial \psi(r, \theta, \phi)}{\partial r} \quad (7)$$

Consider $\omega_r = \omega_\theta = 0$

$$\omega_\phi(r, \theta) = \frac{1}{r} \frac{\partial(rv_\theta)}{\partial r} - \frac{1}{r} \frac{\partial v_r}{\partial \theta} = \frac{\zeta(\psi)}{r \sin \theta} \quad (8)$$

$$\zeta = \frac{\partial^2}{\partial r^2} + \frac{\sin \theta}{r^2} \frac{\partial}{\partial \theta} \frac{1}{\sin \theta} \frac{\partial}{\partial \theta} \quad (9)$$

where ζ is a differential operator with the flow field symmetry outside the sphere having an axial symmetry, i.e. $\partial \phi / \partial \phi = 0$. In other words, here is $V_\phi = 0$ (V_ϕ is component in spherical coordinates) and it behaves like a cylindrical coordinate system due to symmetry. Evaluation of physical boundary around the sphere surface results in:

$$v_r(a, \theta) = 0 \quad (10)$$

$$v_\theta(a, \theta) = 0 \quad (11)$$

Which indicates zero speed on the sphere surface and a long distance from the sphere surface; it can be stated that:

$$v_r(r \rightarrow \infty, \theta) \rightarrow -V \cos(\theta) \quad (12)$$

$$v_\theta(r \rightarrow \infty, \theta) \rightarrow -V \sin(\theta) \quad (13)$$

According to Equation (5) discussed in literature [16], the specifications of the axial Stokes flow can be expressed by the following equation.

$$\zeta^2(\psi) = 0 \quad (14)$$

By writing the boundary conditions from Equations (4) to (7), one can write:

$$\left. \frac{\partial \psi}{\partial r} \right|_{r=a} = 0, \left. \frac{\partial \psi}{\partial \theta} \right|_{r=a} = 0 \quad (15)$$

$$\psi(r \rightarrow \infty, \theta) \rightarrow \frac{1}{2} V r^2 \sin^2 \theta \quad (16)$$

$$v_r(r, \theta) = -\frac{\cos \theta V r^2}{r^2}, v_\theta = \frac{\sin \theta (V r^2)}{2r} \frac{dr}{dr} \quad (17)$$

Equation (2) can be summarized as follows [16]:

$$\nabla \text{Pr} = -\mu \nabla \times \omega = \mu \nabla \phi \times \nabla(\omega_\phi r \sin \theta) \quad (18)$$

Therefore,

$$\frac{\partial \text{Pr}}{\partial r} = -\frac{3\mu V a \cos \theta}{r^3} \quad (19)$$

$$\frac{\partial \text{Pr}}{\partial \theta} = -\frac{3\mu V a \sin \theta}{2r^2} \quad (20)$$

This means that the pressure distribution in that fluid is:

$$\text{Pr}(r, \theta) = p_0 + \frac{3\mu V a \cos \theta}{2r^2} \quad (21)$$

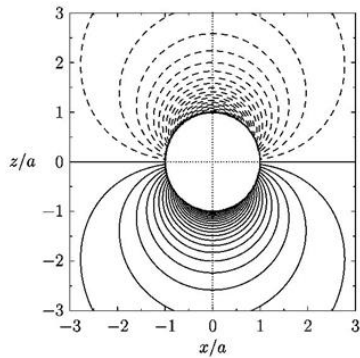
where p_0 is initial pressure Figure 3a shows the axial Stokes flow lines under the influence of the effective pressure on the x-z plane around a solid sphere using Equation (21).

As shown in Figure 3a, each Stokes flow line is affected by constant pressure and velocity in Equation (21); therefore, the parameters Pe , p_0 , V , and μ in Equation (21) are in a fixed line, and hence Equation (21) can be properly converted to an appropriate equation for the barrier's lines.

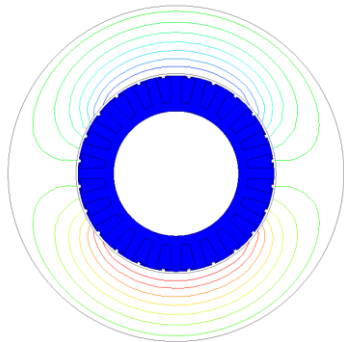
$$C = \frac{\cos(\theta * \frac{p}{2})}{2r^{2p}} \quad (22)$$

$$\theta = \frac{2 * \cos^{-1}(2C.r^{2p})}{p} \quad (23)$$

In the above equations, C is a constant function of the point coordinates through which the curve passes, p is the number of poles. The initial shape of the flux barriers is presented using mathematical equations and parameter C is determined. The results of FEM analysis for the solid rotor and the designed six-pole rotor with three flux barriers are compared in Figure 4. As can be seen, the flux barriers shape is similar to the flux lines shape in the solid rotor. It should be noted that this step,



(a)

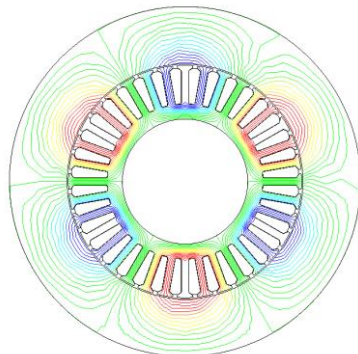


(b)

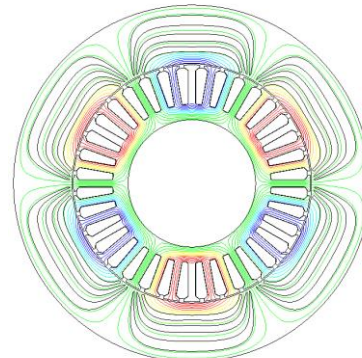
Figure 3. (a) Stokes under pressure $P-p_0$ around a sphere, (b) Magnetic flux line in the external rotor SynRM whit two poles without flux barriers

i.e. designing the flux barriers, is the starting point for rotor design to achieve an optimal design with the least number of simulations. Figures 3b and 4a depict the flux lines in the solid rotor when there are no barriers in the rotor. Since the flux lines in the solid rotor and the fluid pressure lines are similar at equal velocities [16], the fluid velocity and pressure line pattern in fluid mechanics are used to design the flux barriers shape in the external rotor SynRM.

General specifications of the prototype motor suitable for electric scooters are given in Table 1. Design procedure is initiated according to the selected



(a)



(b)

Figure 4. (a) Magnetic flux line in the external rotor SynRM whit six poles without flux barriers, (b) Initial model of the six-pole design with three flux barriers

dimensions in Table 1. Based on the rotor flux lines shape and Equations (22) and (23), the general sketch of the proposed rotor output with the k number of flux barriers is shown in Figure 5.

The angle is equal to $\pi/2p$ along the q -axis, where p is the number of the rotor pole pairs. The position of $Bk_1, Bk_2, \dots,$ and Bk_n (Bk_i in which B and k denote the barrier and the selected flux barriers number, respectively) along the q -axis can be determined by Equations (25)-(31).

Definition of the parameters for determining the size and position of flux barriers in the external rotor is as follows: g is the air gap length, S_i is the iron parts thickness in each section, WB_k is the K th barrier width, B_K is the flux barriers initial and end points on the q -axis, and β is a constant value that determines the flux barrier's arc length.

Selecting insulation ratio in the q -axis (k_{wq} , which is defined as the ratio of the thickness of total insulation

TABLE 1. General specifications of the designed motor

Parameter	Definition	Value
R_{sh}	Shaft outer diameter	20 mm
R_{St}	Stator outer diameter	120.5 mm
R_{Or}	Rotor outer diameter	168 mm
R_{inr}	Rotor outer diameter	121 mm
L	Stack Length (L Stack)	40 mm
P_o	Power	290 W
N	Number of turns	29turns/slot
N_s	Rated Speed	1500 rpm
I	Rated current	6 A
P	Number of pole pairs	3
η	Efficiency	0.84
g	Air-gap width(g)	0.5 mm

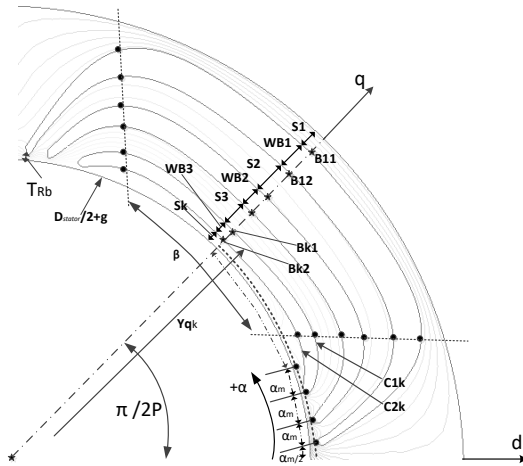


Figure 5. General rotor layout

over total iron conducting material inside the rotor) is the most fundamental and effective part in the rotor design which is defined in literature [17-19]:

$$k_{wq} = \frac{((R_{rotor} - R_{shaft}) - \sum_{n=1}^{k+1} S_i)}{\sum_{n=1}^{k+1} S_i} \quad (24)$$

The initial design is done by selecting the insulation ratio, and the tangential ribs T_{Rb} , shown in Figure 5, are decided according to the practical values which are 0.5 and 0.25mm.

Equation (22) pertains to the calculation of the C_{1k} and C_{2k} potential curves of the flux barrier edges with the starting point of B_{ki} on the q-axis. The flux barriers width and iron parts along the q-axis can be calculated through the equations shown in as follows [18].

$$\frac{WB_k}{WB_m} = \frac{\Delta f_k}{\Delta f_m} \sqrt{\frac{S_k}{S_m}} \quad (25)$$

$$\Delta f_k = f_{q+1} - f_{qk} \quad (26)$$

The gaps between the flux barriers, displayed as S_k , can be calculated by Equation (30), where f_{dh} is the magneto-motive force along the d-axis [19].

$$\frac{2S_1}{S_2} = \frac{fd_1}{fd_2}, \frac{S_h}{S_{h+1}} = \frac{fd_h}{fd_{h+1}}, h=1,2,..k \quad (27)$$

The magneto-motive force (MMF) along the d-axis in each section is equal to the average magnetic driving force by that piece. Therefore, f_{dk} can be calculated through averaging the magneto-motive force between the two end-points of the kth piece; the calculations can be found in literature [18]. The flux barriers width along

the q-axis can be considered W_{BK} [19].

$$\frac{WB_h}{WB_{h+1}} = \left(\frac{\Delta f_h}{\Delta f_{h+1}} \right)^2, h=1,2,..k-1 \quad (28)$$

$$\sum_{h=1}^k WB_h = l_a = \frac{(r_{out} - 2r_{in} - g)}{1 + \frac{1}{k_{wq}}} \quad (29)$$

where Δf_k is the difference between the average MMF per unit and $\sin(p\alpha)$ is the coverage over the Kth barrier in which p is the number of the rotor pair poles. As in Equations (30) and (31), the flux barriers width along the q-axis is, directly and indirectly, a function of k_{wq} , and f_{dh} is the average MMF of the hth piece from MMF_d. According to literature [19] for the best insulation distribution, i.e. the flux barriers width, the flux barriers should have a constant and equal permeability; therefore:

$$\frac{p_i}{p_j} = (cte.) = 1 \Rightarrow \frac{W_{bi}}{W_{b1}} = \left(\frac{\Delta f_i}{\Delta f_1} \right)^2, i=1,2,..,k \quad (30)$$

$$\Delta f_i = f_{qi+1} - f_{qi} \quad (31)$$

By determining the flux barriers width and the gap between the barriers along the q-axis, the radius of a point with the q-axis angle of one of the potential curves is defined and the potential curve can be plotted from the q-axis to the rotor end edge using Equations (22) and (23) and calculation of the C constant.

The initial values of the motor design and dimensions are considered as input parameters. Then, using the Equation (23) expressed in this part, the shape of flux barriers and the positions of the flux barrier in the q axis are determined. Accordingly, the number of flux barriers is selected based on FEM analysis. Consequently, the initial rotor is designed using the Equations (24)-(31). As shown in Figure 2 in the next step, finally, the appropriate parameters for rotor optimization are selected and the rotor is optimized.

3. FEM ANALYSIS RESULT

This section pertains to FEM analysis of the effect of three parameters on the SynRM performance. Each analysis is performed separately to show better insight into the impact each parameter contributes to the torque production. In the last part of this section, the effect of flux barriers number on the rotor is assessed using the results of finite element analysis, and the number of flux barriers is determined for the rotor.

3. 1. Effect of q-axis Insulation Ratio on the Torque Production

The effect of insulation ratio in the q-axis (k_{wq}) on the average torque and torque ripple of the selected external rotor SynRM with six poles in a rotor with one flux barrier and the constant β is considered in the above equations, the results of which are shown in Figure 6. As can be seen, the maximum torque (2.2 N.m) and with peak to peak torque ripple of 1.3(N.m) value is related to $k_{wq}=0.7$.

3. 2. Effect of the Flux Barriers Arc Length on the Torque Production

The effect of changing of the flux barriers arc length (β) on the average torque and peak to peak torque ripple, when k_{wq} is set to the optimal value ($k_{wq}=0.7$), is shown in Figure 7.

As shown in Figure 7, $\beta = 3$ is the best choice for a rotor with one flux barrier, resulting in the maximum average of 2.2 (N.m) torque and the minimum torque ripple of 1.38 (N.m). It is worth mentioning that higher amounts of β may lead to flux barriers interference.

3. 3. Effect of the Number of Flux Barriers on the Torque Production

The effect of the number of flux barriers for a special external rotor SynRM on

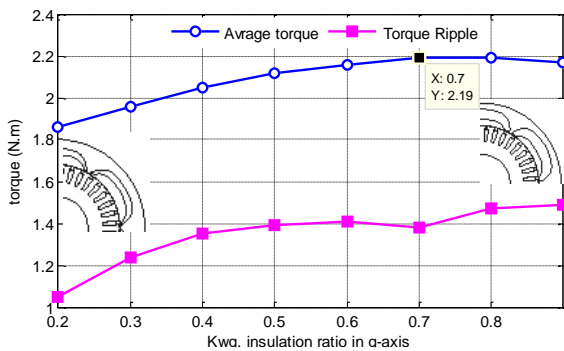


Figure 6. Average Torque and peak to peak torque ripple for different values of k_{wq} for a special β

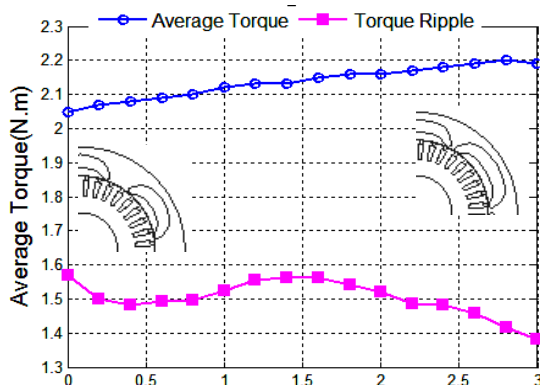


Figure 7. Torque and peak to peak torque ripple (FEM) for different values of β when k_{wq} is 0.7

average torque and torque ripple should be investigated because all design parameters can be affected. For the preliminary study, the calculated optimal values of the q-axis insulation ratio and the optimal arc length coefficient are assumed equal for all cases. Then, a motor with already mentioned characteristics is analyzed with equal parameters and different numbers of flux barriers through the finite element method, the results of which are depicted in Figure 8.

According to the results and considering the average torque and torque ripple values at the same time, a rotor with two flux barriers is the most logical and simplest choice.

4. MULTI-OBJECTIVE OPTIMIZATION OF THE EXTERNAL ROTOR SYNRM

In order to optimally design the motor, the main effective parameters should be analyzed simultaneously. The design variables in this study are the insulation ratio in the q-axis (k_{wq}), the flux barriers arc length (β), the flux barriers width (ΔWB), the displacement of the flux barrier center from the motor shaft center (ΔYq), and the magnetic thickness of the rib from the rotor edges (TRb) as shown in Figure 5.

In this design, the average amounts of torque and torque ripple are considered as the main goals in the fitness function, when the percentage of torque ripple can be expressed as follows:

$$T_R \% = \frac{(T_{Max} - T_{min})}{T_{ave}} \cdot 100 \tag{32}$$

Where T_{Max} , T_{min} , and T_{ave} are the maximum torque, minimum torque, and average torque, respectively. The Taguchi method involves the following steps [20]: (a) defining the number of levels of factors, (b) choosing the number of factors, (c) selecting a suitable orthogonal array and construct the matrix, (d) calculating signal-to-noise (S/N) ratio, (e) analysis of Variance (ANOVA),

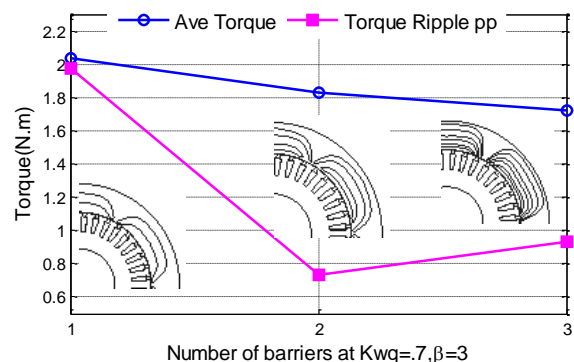


Figure 8. Average torque and torque ripple (FEM) for different values of k , where k is the number of barriers

(f) identifying the control factors and their levels, and (g) analysis of the results. Therefore, Taguchi method involves the identification of proper control factors to obtain the optimum results of the process. According to Figure 5, the rotor with two flux barriers is selected, resulting in 9 parameters for optimization. This experiment has 9 variables at 3 different levels which are shown in Table 2.

A full factorial experiment would require $3^9 = 19683$ combinations of factor levels which takes long time to analyze all the cases. To overcome this problem, Taguchi suggested a special method to take the effects of all mentioned states into consideration in less time to consider all conditions called orthogonal array. The experiment is arranged as $L27 = (3^9)$ in which L represents an orthogonal table with 27 scenarios consisted of nine variables having three levels, the details of which are shown in Table 3.

After performing the experiments according to the orthogonal scenarios, mean effects of optimization parameters on the average torque and torque ripple are plotted.

The type of the control functions related to S/N are “large is the better” and “smaller is the better” for the average torque and torque ripple, respectively [21].

TABLE 2. The levels of design variables

Variable	Level 1	Level 2	Level 3
k_{wq}	0.5	0.6	0.7
ΔY_{q1} (mm)	-2	0	+2
ΔY_{q2} (mm)	-2	-1	0
ΔWB_1 (mm)	-1	0	1
ΔWB_2 (mm)	-1	0	1
β_1 (°)	0	1.5	3
β_2 (°)	0	1.5	3
ΔTR_{b1} (mm)	0.25	0.5	1
ΔTR_{b2} (mm)	0.25	0.5	1

TABLE 3. Experimental plan of L27

N o.	k_{wq}	ΔY_{q1}	ΔY_{q2}	ΔW_{B1}	ΔW_{B2}	β_1	β_2	ΔTR_{b1}	ΔTR_{b2}
1	1	1	1	1	1	1	1	1	1
2	1	1	1	1	2	2	2	2	2
3	1	1	1	1	3	3	3	3	3
.....									
25	3	3	2	1	1	3	2	3	2
26	3	3	2	1	2	1	3	1	3
27	3	3	2	1	3	2	1	2	1

Typical mean effect plots of parameters with respect to torque and torque ripple for motors are shown in Figure 9. As it can be seen, for achieving the maximum torque, the best combination is as follows: 1^{set} level of ΔWB_2 , β_2 , ΔTR_{b1} and ΔTR_{b2} , 2^{set} level of ΔY_{q1} , ΔY_{q2} and β_1 , and 3^{set} level of k_{wq} and ΔWB_1 .

Considering Figure 9b, Minimum torque ripple is obtained as follows: 1^{set} level of k_{wq} and ΔTR_{b2} , 2^{set} level of ΔY_{q1} , ΔWB_1 , β_1 and ΔTR_{b1} , 3^{set} level ΔY_{q2} , ΔWB_2 , β_2 .

Using ANOVA can be useful to determine the effect of input parameter on output results. Then, according to Equations (33) to (35), the sum of the squares of each factor can be calculated [20-22]:

$$T = \sum_{i=1}^n y_i \tag{33}$$

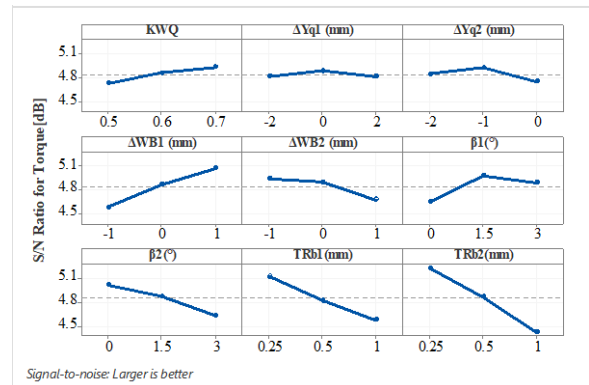
$$SS_A = \frac{1}{t} \sum_{i=1}^m A_i^2 - \frac{T^2}{n} \tag{34}$$

$$SS_T = \sum_{i=1}^n y_i^2 - \frac{T^2}{n} \tag{35}$$

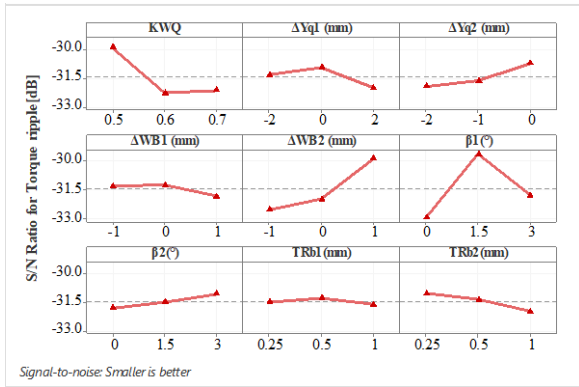
where m is the number of levels of factor A , n is the total number of tests performed, A_i is the sum of the outputs corresponding to the i th level of factor A , t is the number of tests performed at the i th level of factor A , T is equal to the total output of all tests, y_i is the output of the i th test, and SS_T is the sum of all squares.

The effects of the impact weight of all design variables on the desired output obtained through calculations are presented in Table 4.

The selection of appropriate levels of variables is done by comparing the S/N analysis results shown in Figure 9 and the results obtained in Table 3. Then, the optimization variables are selected to achieve the best design results for both average torque and torque ripple. Consequently, 1^{set} level of k_{wq} , β_2 , TR_{b1} , and TR_{b2} , 2^{set} level of ΔY_{q1} and β_1 , and 3^{set} level of ΔY_{q2} , ΔWB_1 , and ΔWB_2 .



(a)



(b)

Figure 9. S/N ratio of the optimization parameters for: (a) average torque, (b) torque ripple

TABLE 4. Impact weight of design variables

Variable	Impact weight on average torque	Impact weight on average torque ripple
k_{wq}	2.41%	20.55%
ΔY_{q1}	0.27%	5.66%
ΔY_{q2}	1.89%	5.82%
ΔWB_1	14.82%	1.28%
ΔWB_2	4.90%	24.34%
β_1	7.55%	34.08%
β_2	9.02%	0.80%
ΔTR_{b1}	19.44%	0.93%
ΔTR_{b2}	39.70%	6.53%

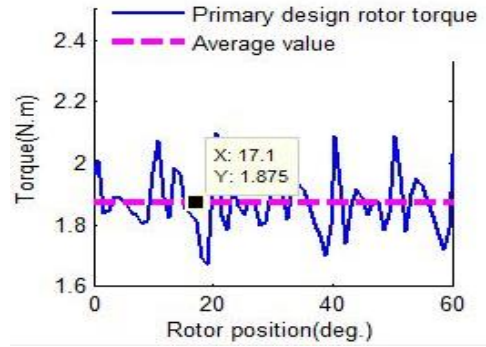
The comparison of the optimized motor with the initial design is presented in Table 5. It is worth mentioning, the variable k_{wq} is set to 0.5, TR_{b1} and TR_{b2} are set to 0.25 mm and the other variables are set to zero for the initial design.

As shown in Figure 10, it is obvious that the optimization of the external rotor motor, with 9 simultaneous effective variables and an acceptable number of tests, is performed well. Accordingly, the primary average torque and torque ripple are improved by 2.6% and 17.7%, respectively.

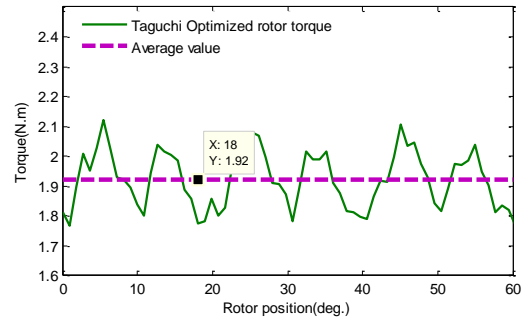
The magnetizing inductances along the d and q axes are the most important parameters in creating torque of the SynRM. As Figure 11 shows by increasing the air gap length L_d decreases while due to the presence of flux barriers in the q axis L_q remains unchanged.

TABLE 5. Comparison of the initial and optimized motors

Definition	Primary motor	Optimized motor
Ave. Torque (N.m)	1.87	1.92
Torque ripple (%)	22.62%	18.61%



(a)



(b)

Figure 10. Torque of Ex-SynRM (a) primary design, (b) Optimized by Taguchi method

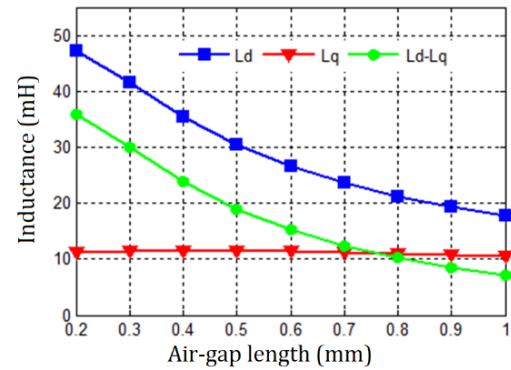


Figure 11. Effect of air-gap on the inductances of Ex-SynRM

Figure 12 shows the maximum flux density on the stator at the rated current is 1.5 Tesla, which is lower than 1.7 Tesla.

5. THE PROTOTYPED MOTOR AND THE EXPERIMENTAL RESULTS

Experimental verification the results of the initial test and a prototype motor with the same dimensions of the optimal design are presented in this section. Figure 13 shows the rotor and stator laminations of the manufactured motor.

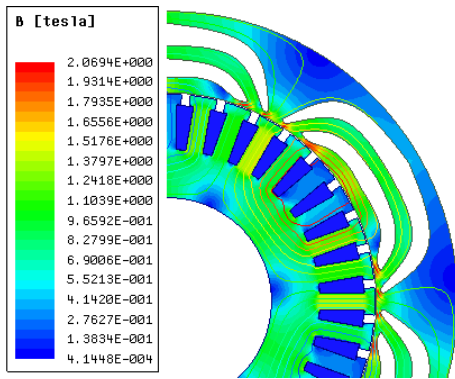


Figure 12. Flux density on the stator and rotor of Ex-SynRM

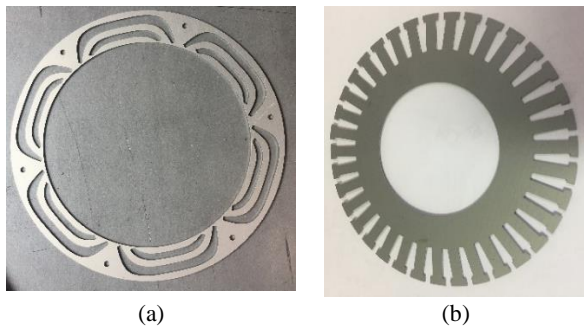


Figure 13. The laminations of (a) rotor and (b) stator

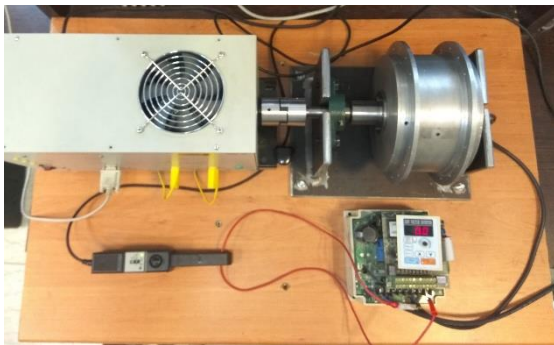


Figure 14. The experimental setup for testing the prototype external rotor SynRM

A 0.3 kW motor is constructed in this study as a prototype motor. The motor is tested in a test setup (shown in Figure 14) equipped with the ABB ACS140 Multi drive system where the current electric angle is 50 degrees. The results of the FEM analysis and measured comparisons are given in Table 7 and Figure 15. The torque measured with FEM is almost the same. The copper loss difference between the practical test and the FEM analysis can be attributed to the difference between the estimated current and the amount required for torque generation of the shaft in the practice. Regarding the iron loss difference, the lamination manufacturing and wire cutting, the accuracy of the rotor and stator assembly processes can be pointed out.

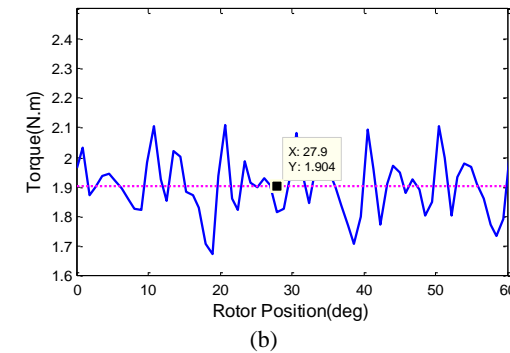
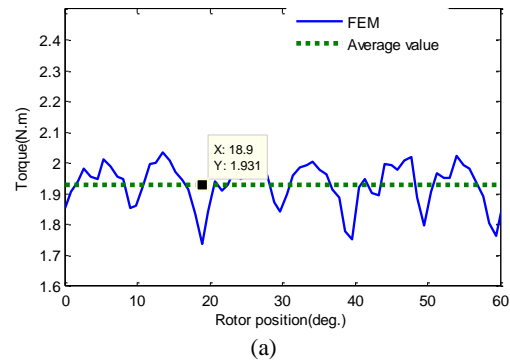


Figure 15. Torque of Ex-SynRM (a) FEM result, (b) Experimental result

TABLE 7. Comparison of the simulation results and experimental results

Definition	FEM	measurement
Ave. Torque (N.m)	1.93	1.90
Torque ripple (%)	22%	23%
Pout (W)	303	294
$\eta\%$	76	71.5
PCu (W)	48.4	56.2
PF	0.74	0.69

Finally, in order to be more accurate in practical results, more specific experiments are needed to accurately examine the core losses and the mechanical losses which data were lost during the experiments.

6. CONCLUSION

The present study proposes a new method for designing an external rotor SynRM. Given the similar behaviors of a fluid around a solid object in fluid mechanics and electromagnetic magnetic flux lines and duality relations between fluid pressure lines and potential electric lines, some simplified equations were provided for further predicting the flux lines in external rotor

reluctance synchronous motors. In the next step, considering the concept of reluctance in SynRMs, certain parameters are considered in the presented equations for controlling the position and shape of the flux barriers in the rotor body. The experiments were performed through Taguchi optimization method using the FEM analysis of an external rotor SynRM. Finally, the selected cases are analyzed and an appropriate rotor model was identified and designed for use in electric scooters. The proposed method is applied for construction of a motor which confirmed through comparing the measured practical results and the design procedure.

7. REFERENCES

- Boglietti, A., Cavagnino, A., Pastorelli, M., and Vagati, A.: 'Experimental comparison of induction and synchronous reluctance motors performance', Fourtieth IAS Annual Meeting. Conference Record of the 2005 Industry Applications Conference, Vol. 1, (2005), 474-479. DOI; 10.1109/IAS.2005.1518350.
- Boglietti, A., and Pastorelli, M.: 'Induction and synchronous reluctance motors comparison', 2008 34th annual conference of IEEE industrial electronics, (2008), 2041-2044. DOI; 10.1109/IECON.2008.4758270.
- Sahebjam, M., Sharifian, B., Feyzi, M.R., and Sabahi, M.: 'Novel Unified Control Method of Induction and Permanent Magnet Synchronous Motors', *International Journal of Engineering, Transactions B: Applications* Vol. 32, (2019), pag no. 256-269. DOI; 10.5829/ije.2019.32.02b.11.
- Arehpanahi, M., and Kheiry, E.: 'A New Optimization of Segmented Interior Permanent Magnet Synchronous Motor Based on Increasing Flux Weakening Range and Output Torque (Research Note)', *International Journal of Engineering, Transactions C: Aspects* Vol. 33, No. 6 (2020), 1122-1127. DOI; 10.5829/ije.2020.33.06c.09.
- Chan, C.: 'The state of the art of electric and hybrid vehicles', Proceedings of the IEEE, Vol. 90, (2002), 247-275. DOI; 10.1109/JPROC.2007.892489.
- Zaim, M.E.H.: 'High-speed solid rotor synchronous reluctance machine design and optimization', *IEEE Transactions on Magnetics*, Vol. 45, (2009), 1796-1799. DOI; 10.1109/TMAG.2009.2012824.
- Kolehmainen, J.: 'Synchronous reluctance motor with form blocked rotor', *IEEE Transactions on Energy Conversion*, Vol. 25, (2010), 450-456. DOI; 10.1109/TEC.2009.2038579.
- Taghavi, S.M., and Pillay, P.: 'A mechanically robust rotor with transverse laminations for a wide-speed-range synchronous reluctance traction motor', *IEEE Transactions on Industry Applications*, Vol. 51, (2015), 4404-4414. DOI; 10.1109/TIA.2015.2445819.
- Aghazadeh, H., Afjei, E., and Siadatan, A.: 'Sizing and detailed design procedure of external rotor synchronous reluctance machine', *IET Electric Power Applications*, Vol. 13, (2019), 1105-1113. DOI; 10.1049/iet-epa.2018.5802.
- Deshpande, Y., and Toliyat, H.A.: 'Design of an outer rotor ferrite assisted synchronous reluctance machine (Fa-SynRM) for electric two-wheeler application', IEEE energy conversion congress and exposition (ECCE), (2014), 3147-3154. DOI; 10.1109/ECCE.2014.6953828.
- Sankestani, M.M.R., and Siadatan, A.: 'Design of outer rotor synchronous reluctance motor for scooter application', 2019 10th International Power Electronics, Drive Systems and Technologies Conference (PEDSTC), (2019). 132-137. DOI; 10.1109/PEDSTC.2019.8697636.
- Moghaddam, R.-R., and Gyllensten, F.: 'Novel high-performance SynRM design method: An easy approach for a complicated rotor topology', *IEEE Transactions on Industrial Electronics*, Vol. 61, (2013) 5058-5065. DOI; 10.1109/TIE.2013.2271601.
- Moghaddam, R.-R.: 'Design optimization of SynRM with Ladybird rotor', 2017 International Conference on Optimization of Electrical and Electronic Equipment (OPTIM) & 2017 Intl Aegean Conference on Electrical Machines and Power Electronics (ACEMP), (2017), 317-323. DOI; 10.1109/OPTIM.2017.7974990.
- Dziechciarz, A., and Martis, C.: 'Magnetic equivalent circuit of synchronous reluctance machine', ELEKTRO, (2016), 500-503. DOI; 10.1109/ELEKTRO.2016.7512126.
- Rajabi Moghaddam, R.: 'Synchronous reluctance machine (SynRM) in variable speed drives (VSD) applications', KTH Royal Institute of Technology, 2011
- Fitzpatrick, R.: 'Theoretical fluid mechanics' (2017). DOI; 10.1088/978-0-7503-1554-8.
- Moghaddam, R.R., Magnussen, F., and Sadarangani, C.: 'Theoretical and experimental reevaluation of synchronous reluctance machine', *IEEE Transactions on Industrial Electronics*, Vol. 57, (2009), 6-13. DOI; 10.1109/TIE.2009.2025286.
- Aghazadeh, H., Afjei, E., and Siadatan, A.: 'Comprehensive Design Procedure and Manufacturing of Permanent Magnet Assisted Synchronous Reluctance Motor', *International Journal of Engineering, Transactions C: Aspects* Vol. 32, No. 9 (2019),. 1299-1305. DOI; 10.5829/ije.2019.32.09c.10. 1.
- Moghaddam, R.R., Magnussen, F., and Sadarangani, C.: 'A FEM 1 investigation on the Synchronous Reluctance Machine rotor geometry with just one flux barrier as a guide toward the optimal barrier's shape', IEEE EUROCON, (2009), 663-670. DOI; 10.1109/EURCON.2009.5167704.
- Ajamloo, A.M., Ghaheri, A., and Afjei, E.: 'Multi-objective Optimization of an Outer Rotor BLDC Motor Based on Taguchi Method for Propulsion Applications', 2019 10th International Power Electronics, Drive Systems and Technologies Conference (PEDSTC), (2019), 34-39. DOI; 10.1109/PEDSTC.2019.8697586.
- Arkadan, A., and Al Aawar, N.: 'Taguchi-EM-AI Design Optimization Environment for SynRM Drives in Traction Applications', International Applied Computational Electromagnetics Society Symposium (ACES), (2020). 1-2. DOI; 10.23919/ACES49320.2020.9196111.
- Mansoursamaei, M., Hadighi, A., and Javadian, N.: 'A New Approach Applying Multi-Objective Optimization using a Taguchi Fuzzy-based for Tourist Satisfaction Management', *International Journal of Engineering, Transactions C: Aspects* Vol. 32, (2019), 405-412. DOI; 10.5829/ije.2019.32.03c.08.

Persian Abstract

چکیده

موتور سنکرون رلوکتانسی یک موتور اقتصادی با عملکرد در محدوده وسیع سرعت می‌باشد. اما به طور عمومی ریپل گشتاور این نوع از موتورها به دلیل تغییر مقاومت مغناطیسی بین موانع شار و دندانه استاتور قابل ملاحظه است. دستیابی به طراحی بهینه یک ماشین سنکرون رلوکتانسی از میان تمامی ترکیب‌های ممکن روتور با اشکال مختلف موانع شار و بدون استفاده از روابط تئوری ریاضی و الگوریتم مشخص طراحی کاری بسیار زمان‌بر است. در این مطالعه یک روش جامع برای طراحی روتور موتور سنکرون رلوکتانسی با ساختار روتور بیرونی با شکل موانع شار الگو گرفته شده از رفتار مایعات جاری اطراف یک جسم جامد ارائه شده است. با استفاده از این روش جدید طراحی، یک طرح روتور بیرونی پیشنهاد و در ادامه با استفاده از الگوریتم چند هدفه تاگوچی مبتنی بر تحلیل المان محدود (FEM) با هدف به حداکثر رساندن مقدار متوسط گشتاور و کاهش ریپل گشتاور تولیدی بهینه سازی شده است. در انتها برای اعتبارسنجی صحت نتایج حاصل از شبیه‌سازی های صورت گرفته یک نمونه اولیه از موتور پیشنهادی برای اسکوتر برقی ۳۰۰ وات و ۶ قطب، با روتوری با تعداد دو لایه مانع مغناطیسی و با استاتور ۳۶ شیار همراه با سیم پیچی توزیع شده ساخته شده است. مقایسه نتایج عملی به خوبی درستی نتایج شبیه‌سازی را تأیید می‌کند.
